A new Arctic MSS model derived from combined Cryosat-2 and ICESat observations

Chen, Guodong; Zhang, Zhijie; Rose, Stine Kildegaard; Andersen, Ole Baltazar; Zhang, Shengjun; Jin, Taoyong

Published in:
International Journal of Digital Earth

Link to article, DOI:
10.1080/17538947.2022.2153181

Publication date:
2022

Document Version
Publisher's PDF, also known as Version of record

International Journal of Digital Earth

ISSN: (Print) (Online) Journal homepage: https://www.tandfonline.com/loi/tjde20

A new Arctic MSS model derived from combined Cryosat-2 and ICESat observations

Guodong Chen, Zhijie Zhang, Stine Kildegaard Rose, Ole Baltazar Andersen, Shengjun Zhang & Taoyong Jin

To cite this article: Guodong Chen, Zhijie Zhang, Stine Kildegaard Rose, Ole Baltazar Andersen, Shengjun Zhang & Taoyong Jin (2022) A new Arctic MSS model derived from combined Cryosat-2 and ICESat observations, International Journal of Digital Earth, 15:1, 2202-2222, DOI: 10.1080/17538947.2022.2153181

To link to this article: https://doi.org/10.1080/17538947.2022.2153181

Published online: 07 Dec 2022.

INTERNATIONAL JOURNAL OF DIGITAL EARTH
2022, VOL. 15, NO. 1, 2202–2222
https://doi.org/10.1080/17538947.2022.2153181

RESEARCH ARTICLE

OPEN ACCESS Check for updates

A new Arctic MSS model derived from combined Cryosat-2 and ICESat observations

Guodong Chen [a], Zhijie Zhang[a], Stine Kildegaard Rose[b], Ole Baltazar Andersen[b], Shengjun Zhang[c] and Taoyong Jin[d]

[a]School of Geography Science and Geomatics Engineering, Suzhou University of Science and Technology, Suzhou, People's Republic of China; [b]National Space Institute, Technical University of Denmark, Kongens Lyngby, Denmark; [c]School of Resources and Civil Engineering, Northeastern University, Shenyang, China; [d]School of Geodesy and Geomatics, Wuhan University, Wuhan, People's Republic of China

ABSTRACT

Due to the existence of seasonal or perennial sea ice cover, the determination of the Arctic sea surface is more difficult than that of mid-low latitudinal oceans. Focusing on the sea surface height in the ice-covered region, this paper constructs a new Arctic mean sea surface (MSS) model, named SUST22, by combining the measurements from ICESat and Cryosat-2 missions. The lead detection methods of ICESat and Cryosat-2 are first studied and modified to acquire sea surface measurements with better accuracy. The results have shown that the standard deviation of Cryosat-2-derived Arctic sea surface height is about 3–4 cm in 10-km resolution grids, while the value of ICESat is 5–6 cm. Then the MSS construction procedure is discussed and the SUST22 MSS model is constructed. The new model is compared with the other four Arctic MSS models. The best agreement is found between SUST22 and DTU21 with an average difference of -4.0 ± 5.2 cm. These models are also validated by ICESat-2 samples. The average difference between ICESat-2 and SUST22 is 15.8 ± 7.4 cm, which shows that the new model SUST22 presents better consistency with the ICESat-2 than any of the other models.

ARTICLE HISTORY
Received 18 August 2022
Accepted 22 November 2022

KEYWORDS
Arctic; ICESat; Cryosat-2; MSS; lead detection

1. Introduction

Since the beginning of the satellite altimetry era, both the quantity and quality of observations over the ocean have been significantly improved. For decades, altimetry satellites have provided massive sea surface observations with high accuracy which greatly promote the studies of the mean sea surface, sea level trend, ocean tide and other oceanographic research studies. While a series of high-accuracy global MSS models were established (Wang 2001; Andersen and Knudsen 2009; Schaeffer et al. 2012; Jin, Li, and Jiang 2016), the MSS in ice-covered Arctic ocean had lagged for a long time. There are two major problems for Arctic sea surface observation. First, sea ice hampers the direct observation of sea surface height from space, leading to low data quality in the Arctic in early MSS models (Prandi et al. 2012). Second, the latitudinal coverages of satellites were limited by their inclination angles, which leads to that only a few altimetry satellites can fly over the Arctic and just part of the Arctic Ocean can be observed.

CONTACT Zhijie Zhang zjzhang@shao.ac.cn School of Geography Science and Geomatics Engineering, Suzhou University of Science and Technology, No. 99, Xuefu Road, Huqiu District, Suzhou City, Jiangsu Province, Zip code: 215009, People's Republic of China

However, sea surface elevations are still possible to be acquired by those altimetry observations from the cracks between sea ice floes, known as leads. The first Arctic sea surface model was constructed by ERS-1/2 data (Peacock and Laxon 2004). This result demonstrated the potential of studying the Arctic sea surface and sea ice by satellite altimetry. After this preliminary attempt, more and more Arctic Ocean research studies were carried out with satellite altimetry data. Early observations of the Arctic Ocean were mainly acquired by conventional radar altimeters, providing indispensable information for Arctic sea level studies. The reliability of the radar altimeter was validated by Connor et al. (2009), which showed an excellent agreement between the lead elevations derived by Envisat and those measured by airborne laser altimetry. Using four altimetry satellites, including GFO, ERS-1/2 and Envisat, Prandi et al. (2012) found the Arctic sea level changed with an average rate of 3.6 ± 1.3 mm/yr during 1993–2009. By the re-process of ERS-1/2 and Envisat data with optimal selection of the reference MSS model, tide model and other geophysical corrections, Cheng, Andersen, and Knudsen (2015) revealed an Arctic sea level trend of 2.1 ± 1.3 mm/yr between 1992 and 2012. Poisson et al. (2018) developed the re-tracking algorithm of Envisat to obtain continuous sea level records between the open ocean and the Arctic, whose results were adopted in Collecte Localization Satellites (CLS) sea level products.

However, the spatial coverage of those conventional radar altimeters was limited by a satellite orbit with a latitudinal limitation of 81.5°N, leaving a large hole in the central Arctic. This situation was changed by NASA's Ice, Cloud, and Land Elevation Satellite (ICESat) laser altimetry mission and ESA's Cryosat-2 radar altimetry mission. These two missions were specially designed for polar investigations, with higher latitudinal coverages of 86°N and 88°N. With the measurements collected by these two missions, the Arctic sea surface was studied more comprehensively. Using ICESat data, Skourup (2009) studied the Arctic MSS and Mean dynamic topography (MDT), and the derived MDT was consistent with the MDT model provided by the University of Washington. Kwok and Morison (2011) also studied Arctic MDT with ICESat and validated the accuracy of their results with hydrographic data. Farrell et al. (2012) created an ICEen Arctic MSS model by combining ICESat and Envisat data and analyzed Arctic MDT by ICEen and EGM2008 geoid. Following Cheng, Andersen, and Knudsen (2015), Andersen and Piccioni (2016) extended the Arctic sea level time-series with Cryosat-2 data and revealed a sea level trend of 2.2 ± 1.1 mm/yr from 1993 to 2015. Armitage et al. (2016) carefully analyzed Arctic sea level variation from radar altimetry and GRACE and found that a large seasonal cycle of Arctic sea surface height was dominated by seasonal steric height variation. Using combined ERS-1/2, Envisat and Cryosat-2 observations, Rose et al. (2019) presented the Arctic sea level record between 1991 and 2018 with an improved re-tracking algorithm, and a sea level rise of 1.54 mm/yr was found. Prandi et al. (2021) presented an Arctic sea level anomaly (SLA) dataset with combined observations from SARAL/AltiKa, Cryosat-2 and Sentinel-3A, exhibiting better performance and temporal resolution than mono-mission datasets. Doglioni et al. (2022) also provided monthly SLA products spanning from 2011 to 2020 with Cryosat-2 products. In addition to sea level, some key technologies of sea surface determination in polar oceans were also widely used in sea ice research, especially with ICESat and Cryosat-2 measurements (see e.g. Kwok et al. (2007), Zwally et al. (2008), Laxon et al. (2013), Lee, Kim, and Im (2018) and Dettmering et al. (2018)).

Due to broad coverage in the Arctic, the laser altimetry mission ICESat and the ku-band radar altimetry mission Cryosat-2 attract our interest. In former studies, the advantages of Cryosat-2 have been proved compared to traditional radar altimeters (Guerreiro et al. 2017; Rose et al. 2019; Tilling, Ridout, and Shepherd 2019). As for ICESat, the 50–70 m size footprint and 40 Hz frequency of the laser altimeter make it possible to provide the precise surface height of lead or thin ice (Kwok and Morison 2011; Farrell et al. 2012). Moreover, the high latitudinal coverages of these two missions allow more comprehensive inspections of the Arctic Ocean. In this paper, the lead detection technologies of both missions were inspected first. Then an Arctic MSS model derived from combined ICESat and Cryosat-2 was established and validated by other four published models and altimetry samples. The paper is organized as follows. After a summary of existing studies in Section 1, a

description of the datasets used in this study is given in Section 2. The extraction of sea surface height from Cryosat-2 and ICESat is introduced in Section 3, and a new Arctic MSS model is constructed by combining the measurements of both missions in Section 4, followed by some discussions in Section 5. The main conclusions are summarized in Section 6.

2. Data description

2.1. Cryosat-2 observations

Cryosat-2 is ESA's first ice mission to monitor variations in the thickness of the polar sea ice covers and continental ice sheets. It was launched on 8 April 2010 and started its data collection in July 2010, with an altitude of about 717 km and a latitudinal coverage of 88°S-88°N. So far, it has already operated for over 11 years and the data are regularly released by ESA. Since a new type of delay/Doppler radar altimeter, SIRAL, is carried on the satellite, Cryosat-2 can operate in three different modes to cope with different surfaces on Earth: Low-Resolution Mode (LRM) for open ocean and interior ice sheets, Synthetic Aperture Radar (SAR) mode for ice-covered polar oceans and Synthetic Aperture Radar Interferometry (SIN) mode for sloping terrains such as the ice sheet margins. In the ice-covered Arctic Ocean, the Cryosat-2 observations are mainly collected using the SAR mode. In this paper, the processing of SAR mode data is discussed. Two types of Cryosat-2 data products were used in this study: the Level-1b waveform product is used for lead detection and the surface elevation from Level-2 Geophysical Data Record (GDR) is used for sea surface determination. Both products can be downloaded from ESA's ftpserver (ftp://science-pds.cryosat.esa.int/). When this study started, the current Baseline D CryoSat-2 products were not available, hence Baseline C products are used in our research and the time span of Cryosat-2 data is from July 2010 to March 2019, consisting of 105 months.

2.2. ICESat observations

The ICESat mission is the first low-earth-orbit satellite with three laser altimeters on board. It NASA launched in January 2003 and stopped its operation in October 2009. Unlike radar altimeters, the laser altimeter had much smaller footprints and did not penetrate the snow, hence it had better accuracy and precision on polar ice (Brenner, DiMarzio, and Zwally 2007). Due to unexpected manufacturing defects of the lasers, ICESat only operated 18 campaigns (about 33 days for each campaign) during 2003–2009. For the sake of simplicity, the ICESat campaigns are identified by the last two digits of the year and the initials of the month in this paper. For example, 03FM represents the campaign operated in February and March 2003. ICESat GLA13 release 34 products are used in our study, which can be downloaded from National Snow and Ice Data Center (NSIDC). Since ICESat data suffered from severe saturation and forward scattering (Zwally et al. 2008), strict data editing is implemented. Any observations with more than one peak, reflectivity higher than 1.0 or lower than 0.05, or pulse broadening parameter larger than 0.8 (Zwally et al. 2008) are removed. Due to the energy decline of the lasers (Abshire et al. 2005), most of the observations collected in campaigns 04MJ, 08O, 08ND, 09MA and 09SO were rejected by our data-editing approach. Therefore, these five campaigns are not involved in our research, and consequently, the time span of ICESat data in this paper is between February 2003 and March 2008, consisting of 13 campaigns.

2.3. Current Arctic MSS models

Four widely used MSS models are compared with each other in the Arctic Ocean in this paper: DTU21, CLS2015, WHU2013 and UCL13. The DTU MSS models were developed and published by the Technical University of Denmark, and DTU21 was the latest version (Andersen et al. 2021). The CLS MSS models were developed by Centrale Nationale d'Etudes Speciales (Schaeffer

et al. 2012) and published by AVISO, and CLS2015 was the latest version available on the AVISO website. The WHU2013 was developed by Wuhan University (Jin, Li, and Jiang 2016) and can be acquired from the author. These three models were all derived from ERS-1/2, Envisat and Cryosat-2 inside the Arctic circle (Skourup et al. 2017; Sun et al. 2021) but they had different spatial coverages. The 2' resolution DTU21 and WHU2013 models and the 1' resolution CLS2015 model were acquired in this paper. While the DTU21 MSS covers the whole Arctic Ocean, the CLS2015 and WHU2013 have a latitudinal limitation of 84°N. The UCL13 MSS was developed by University College London and provided for Cryosat-2 users since Baseline C products were published. The model was derived from two complete cycles of Cryosat-2 north of 60°N (Skourup et al. 2017), hence the spatial coverage can reach 88°N. We extracted UCL13 MSS values from the Cryosat-2 Level-2 GDR product and converted them into regular 2'×2' grids using bilinear interpolation with ArcGIS. In addition, the CLS2015 MSS was also resampled into 2'×2' grids to facilitate direct comparison between different models.

2.4. Other data/model

ICESat-2 altimetry, Moderate-Resolution Imaging Spectroradiometer (MODIS) image and Earth Gravitational Model (EGM2008) are also used in this paper. As the successor of ICESat, ICESat-2 was launched on September 15th, 2018. With a photon-counting laser altimeter on board, ICESat-2 collects high-resolution height observations from 88°S to 88°N. ICESat-2 Arctic/Antarctic sea ice elevation product, ATL07, is used in Section 4.3 to validate the accuracy of Arctic MSS models. MODIS is a remote sensing instrument that acquires images of the Earth's surface in 36 spectral bands, which was on board Aqua and Terra satellites. The 250 m resolution radiance images collected by MODIS are used in Section 3.1 to visually distinguish open leads. EGM2008 is a widely used global geoid model. It is a spherical harmonic model that was completed to degree 2159 and order 2159. This model is used as the reference surface during MSS construction in this study.

3. Extraction of sea surface height

3.1. Lead detection of Cryosat-2

For radar altimeters, lead observations can be separated by waveform classification because radar pulse reflections from different surfaces have different characteristics (Peacock and Laxon 2004). The effectiveness of Cryosat-2 has been proved by many research studies (e.g. Laxon et al. 2013; Ricker et al. 2014; Wernecke and Kaleschke 2015), but different waveform parameters and thresholds were used in different research studies. In this paper, the two most commonly used parameters, Pulse Peakiness (PP) and Stack Standard Deviation (SSD), are used for lead detection. PP is the ratio of the maximum energy of the echo waveform to the average energy of every range gate, which measures how sharply peaked an echo is. Usually, radar altimetry observations from leads are accompanied by large PP values. In this paper, PP is calculated as

$$PP = \frac{256 \cdot \max\left(P^{wf}\right)}{\sum_{i=1}^{256} P_i^{wf}} \tag{1}$$

where P_i^{wf} is the power of the ith range bin provided in the Cryosat-2 L1b product. SSD is the standard deviation of Gaussian fit to range integrated stack power. It provides information on the variation of surface backscattering power with incidence angle (Wingham et al. 2006) and can be retrieved directly in the L1b product. Small values of SSD are usually considered an indicator of lead returns.

The thresholds of the two parameters for lead detection, however, are subjective, and different values are selected by different authors. In this paper, different thresholds were tested for lead

detection, with PP values ranging from 50 to 110 (with a fixed SSD threshold of 4.0) and SSD values from 1.0 to −4.0 (with a fixed PP threshold of 50). In the Arctic, the small-scale sea surface waves are hampered by the sea ice cover (Spreen 2008), and the variation of altimetry measurements is mainly due to the sea ice thickness rather than the sea surface (Kwok et al. 2007). Therefore, the identified measurements in each month were divided into 10-km grids (in this paper, the Equal-Area Scalable Earth (EASE) Grids projection is used for gridding) and the standard deviations of observed surface height were recorded as an indicator of lead detection accuracy. In other words, the standard deviations of surface height during the same month in 10-km grids (abbreviated as δ_{grid} hereafter) derived from Cryosat-2 should be small if the sea ice measurements are completely removed. To minimize the spatial variations caused by static geoid fluctuations, the EGM2008 geoid model is subtracted from altimetry records. Another issue is the data coverage, defined as the number of grids with valid lead observations divided by the total number of grids in the ice-covered Arctic. Skourup et al. (2017) proved that spatial resolution was crucial to Arctic studies such as sea ice thickness, hence high data coverage is expected in this research. Only those grids with at least 5 Cryosat-2 measurements were involved because small samples may lead to accidental errors. The median δ_{grid} values obtained with different thresholds are shown in Figure 1. As expected, for both parameters, Figure 1 has proved that smaller monthly δ_{grid} values were obtained when more stringent thresholds were applied, along with few valid grids. However, the choice of SSD threshold seems to have a relatively smaller effect than PP. From an SSD threshold of 4–2, it has only a δ_{grid} decrease of about 10% (from 4.2 cm to 3.8 cm) and a coverage decrease of about 7% (from 45% to 38%). When smaller SSD thresholds are applied (i.e. SSD < 1.5 and SSD < 1.0), the data coverage has decreased significantly, while the value of δ_{grid} is around 3.7–3.8 cm. This result suggests that an SSD threshold of less than 2 is unnecessary for Cryosat-2 lead detection. In contrast, the threshold of PP has a much greater impact on lead detection. The value of δ_{grid} is obviously improved when the PP threshold is raised from 50 to 90, suggesting that more falsely identified lead observations are rejected. However, very little improvement is observed for δ_{grid} when the PP threshold exceeds 90, yet the data coverage keeps falling dramatically. Therefore, the PP threshold over 90 is also unnecessary.

Furthermore, the two parameters are also inspected by coincident Cryosat-2 data and MODIS images. An example is shown in Figure 2, together with the PP and SSD values of the Cryosat-2 trajectory. Leads or recently formed thin ice can be identified visually as the dark-coloured areas in MODIS images, and the large PP and small SSD characteristics of leads can be confirmed in Figure 2. However, Figure 2 shows that many true leads will be rejected by the thresholds of PP > 90 and SSD < 2.0, indicating these thresholds are actually overcautious for those studies that require a large number of lead observations. By visual identification of coincident Cryosat-2 tracks

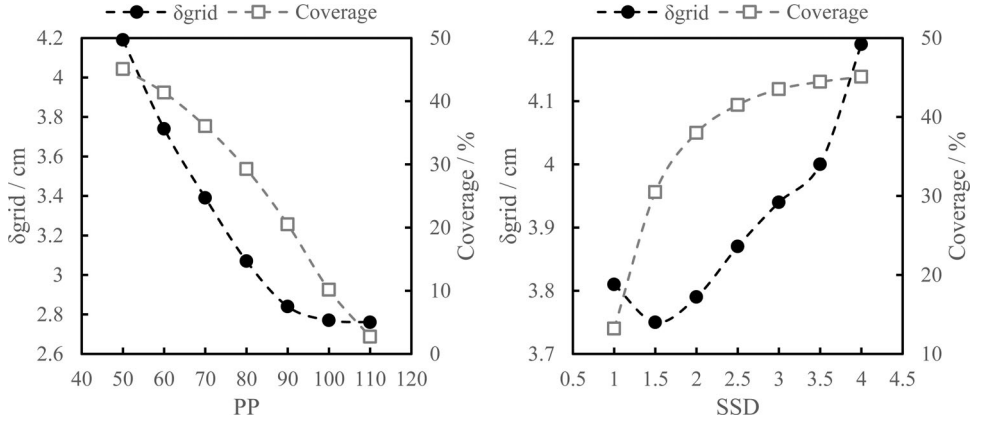

Figure 1. Median standard deviation in 10-km grids and data coverage obtained by different thresholds of PP and SSD.

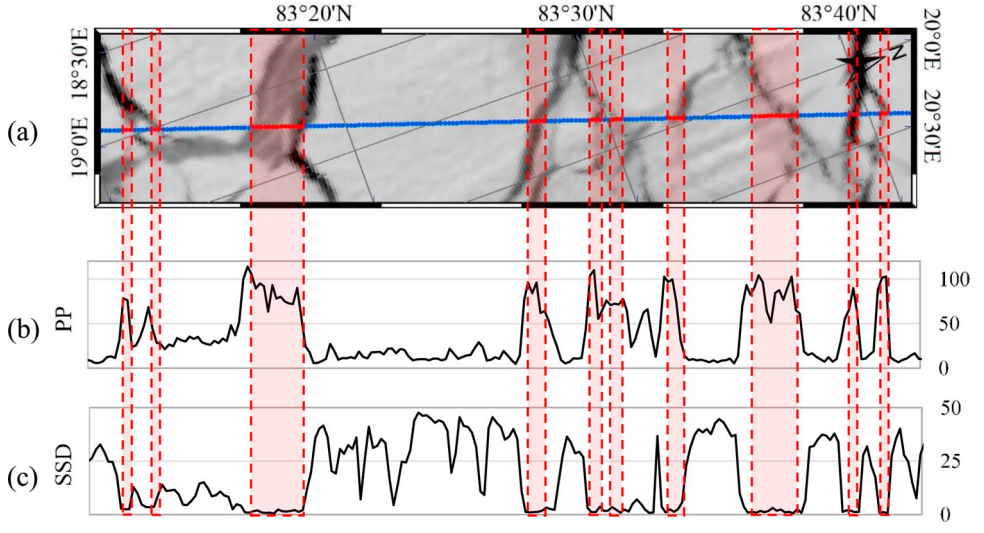

Figure 2. A sample of Cryosat-2profile (observed on 17 April 2014) overlaid on coincident MODIS image (a) and variation of the corresponding PP (b) and SSD (c), the red dots and shaded areas representing leads identified visually.

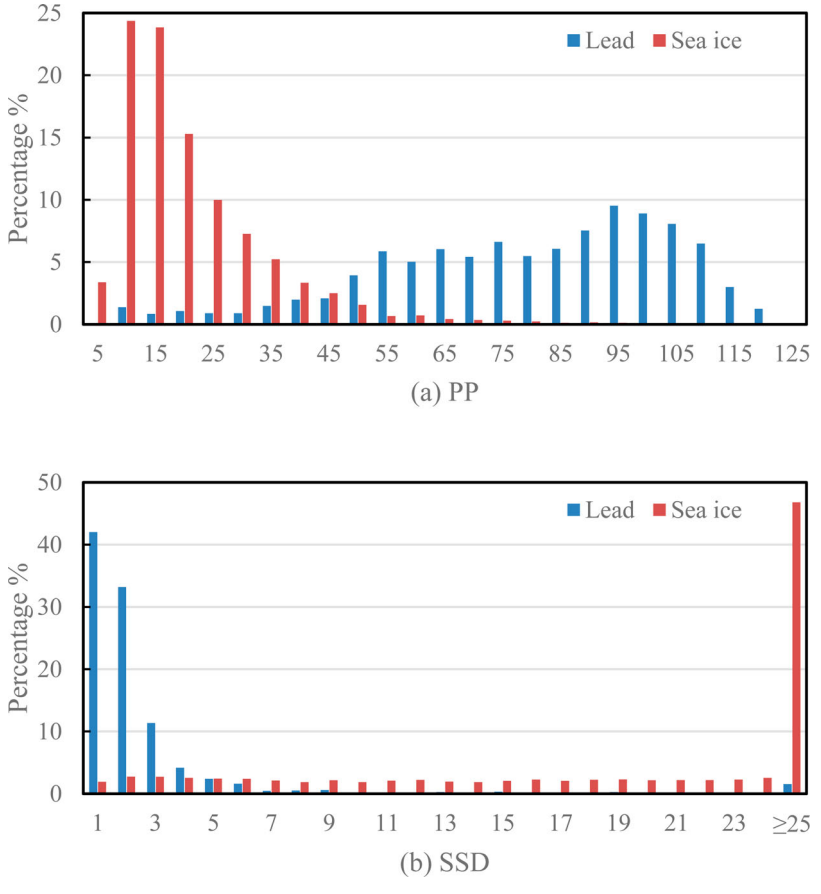

Figure 3. Histograms of PP and SSD of lead and sea ice samples confirmed by visual identification.

and MODIS images, 3580 lead observations and 19,806 sea ice observations are selected as samples represented for each surface type, and the histograms of PP and SSD of different surfaces are shown in Figure 3. According to Figure 3(a), the threshold of PP > 90 can almost reject all the sea ice samples, but it will also reject more than half of the lead samples. The situation is similar when the SSD threshold of 2.0 is applied according to Figure 3(b). Since the high spatial resolution is one of the aims, more moderate thresholds of PP > 70 and SSD < 3.0 are used for lead detection in this paper. According to statistics in Figure 3, over 60% of the lead samples can be correctly identified and only about 1% of sea ice samples will be misidentified as leads by these thresholds.

Then the median δ_{grid} values of Cryosat-2 lead observations in each month are investigated to check if it is affected by seasonal variations, as shown in Figure 4, with thresholds of PP > 70 and SSD < 3.0. The average value is around 3.5 cm. An obvious seasonal pattern can be seen in Figure 4: The δ_{grid} value keeps stable from December to April, and rises afterwards until its top in June or July, then it declines quickly until August and keeps low from August to October, and rises again from October to December. The larger values in June and July may be explained by melt ponds. This melted water on top of sea ice packs cannot be distinguished by radar waveform, hence biases the sea surface height estimation. However, a trough in August, September and October can be seen in Figure 4 although melt ponds still exist in these months. A possible explanation for this is the thinning of sea ice. When the sea ice melts in summer months, the lower sea ice freeboards bring few errors even if observations from melt ponds are misidentified as leads. Conversely, when the ice grows thicker from November to April, the δ_{grid} values increase with higher freeboards, because some sea ice observations might still be misidentified as leads. To further remove these outliers, a height-editing procedure was applied to the identified lead observations. According to the results shown in Figures 1 and 4, the standard deviation of true sea surface height (actually MDT, because the EGM2008 geoid has been subtracted) should be around 3 cm in each 10 km grid when strict thresholds are applied; therefore, those observations are removed as outliers if their height difference with the grid average exceeds 6 cm. This procedure produces δgrid values close to 3 cm but the number of valid grids is not reduced, hence the spatial coverage is ensured.

3.2. Lead detection of ICESat

A lowest-level method was widely used by many researchers for sea surface determination with ICESat. It was first proposed by Forsberg and Skourup (2005) and detailed in Zwally et al. (2008), which was then adopted in many studies of sea ice and sea surface in Arctic and Antarctic Oceans (e.g. Forsberg and Skourup (2005), Spreen (2008), Zwally et al. (2008), Farrell et al. (2012) and Pavlis et al. (2012)). This method assumes that ICESat can certainly detect lead or thin ice in ice-covered oceans only if the observation profile is long enough. With this assumption, the local sea surface height can be determined by the lowest observations of a certain proportion. Obviously,

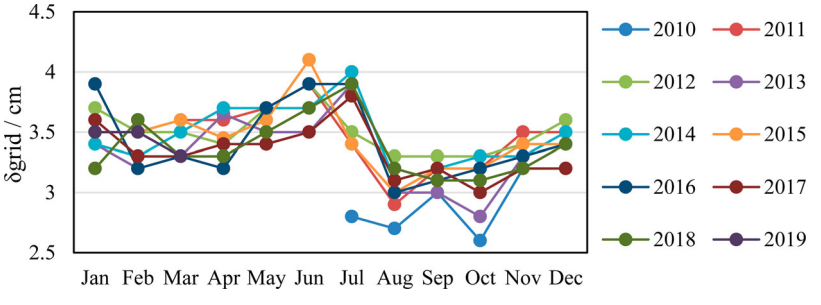

Figure 4. Median standard deviations of Cryosat-2 lead observations in 10-km grids for each month (obtained with PP > 70 and SSD > 3.0).

the local sea surface will be contaminated if the actual lead fraction is less than the proportion used in the lowest-level method. It also brings bias when the actual lead fraction is greater than the lowest-level proportion because this method always tends to select lower measurements, no matter if the observation quality is good or not. However, this method is still favored by many researchers because it can provide sea-level information anywhere in the Arctic and Antarctic ice-covered oceans. Therefore, this method was first estimated with δ_{grid}, as shown in Figure 5 (before modification). In this procedure, 6 of about 290 observations are selected for sea surface height determination along each 50 km ICESat track segment following Zwally et al. 2008, then the value of δ_{grid} is calculated for each campaign instead of calendrical months because ICESat campaigns usually lasted 33 or 34 days, only a little bit more than one month. The grid size is also 10 km the same as Cryosat-2. The δ_{grid} value of the lowest-level method is typically 5–10 cm, which shows a less accurate performance compared with Cryosat-2 (see Figure 1). The first ICESat campaign, 03FM, has an abnormal δ_{grid} value of 14.3 cm, indicating a poor accuracy of this campaign. Besides, δ_{grid} also differs from different campaigns. This is expected because actual lead fractions differ from campaigns while a uniform 2% proportion is used for all campaigns. These results imply that ICESat leads identified by 2% lowest-level are still contaminated by sea-ice observations. Therefore, this method needs to be modified in this study.

Different from Cryosat-2, the height-editing procedure mentioned in Section 3.1 should not be implemented for ICESat-identified 'lead' observations because the lowest-level method itself already has a similar effect. In this paper, waveform parameters were used for ICESat data editing. According to the references (Kwok et al. 2007; Farrell et al. 2009), four waveform parameters, including the uncorrected reflectivity (R), receiver gain (G), pulse broadening (S) (Zwally et al. 2008) and length of received waveform (L), are employed in this paper. The first two parameters can be extracted directly from the GLA13 product and the last two can be calculated as

$$S = \frac{c}{2}\sqrt{\sigma_R^2 - \sigma_T^2} \tag{2}$$

$$L = \frac{c}{2}(t_{\text{siged}} - t_{\text{sigbg}}) \tag{3}$$

where σ_T and σ_R are the pulse widths of transmitted and received waveform t_{sigbg} and t_{siged} are the start and end time of the received signal, respectively, c denotes the speed of light. Theoretically, specular reflections on leads can lead to much smaller values for all four parameters than sea ice reflections

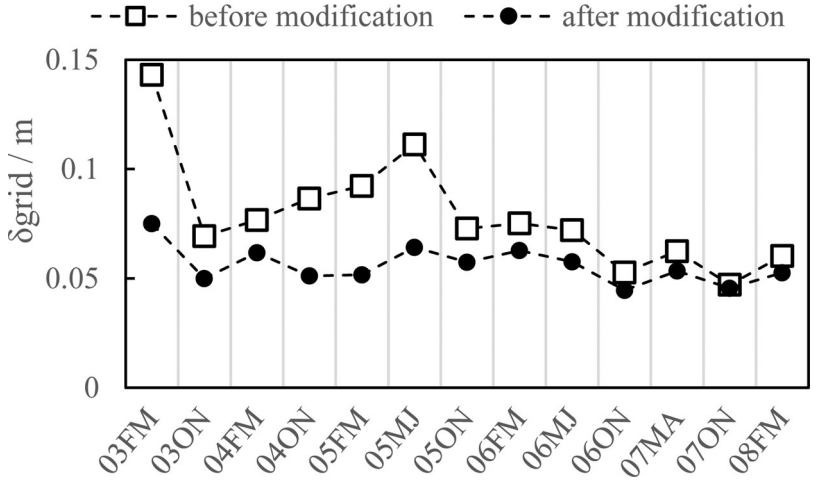

Figure 5. Median standard deviations in 10-km grids of each ICESat campaign, before and after modification.

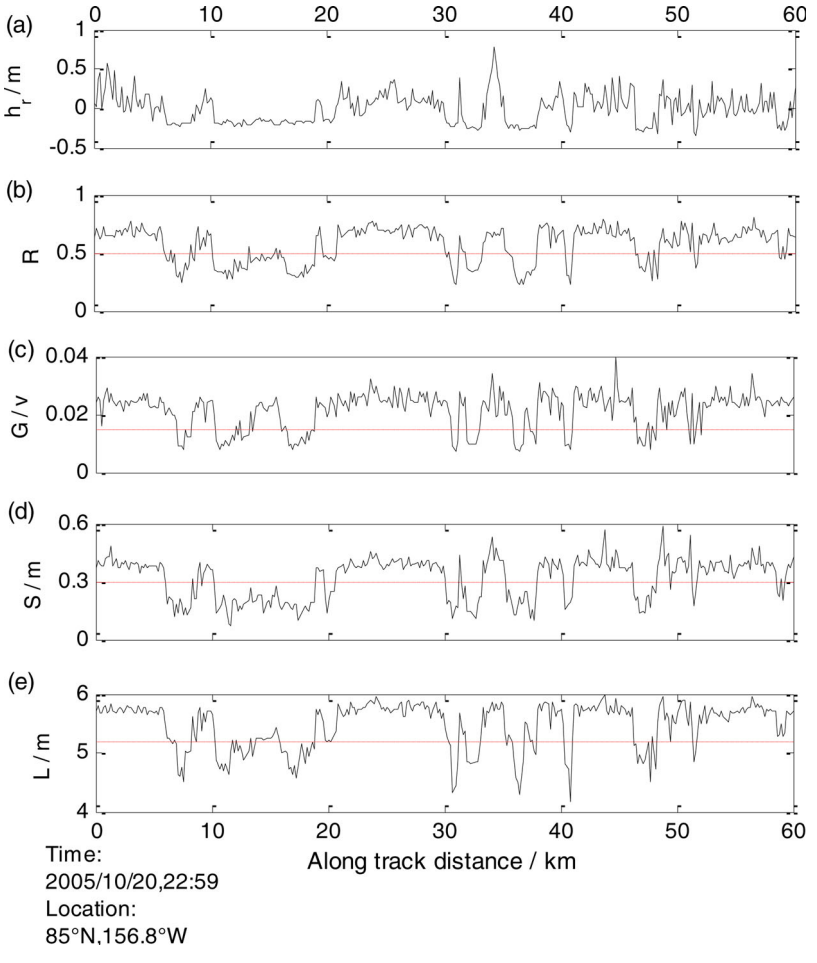

Figure 6. A sample of ICESat profile with corresponding detrended elevation (a), reflectivity (b), receiver gain (c), pulse broadening (d) and waveform length (e), along with the thresholds for each parameter (red dashed lines).

(Kwok et al. 2007; Zwally et al. 2008; Farrell et al. 2009). By the visual inspection of ICESat data (see sample data in Figure 6), those observations with $R < 0.5$, $G < 0.15$, $S < 0.3$ and $L < 5.2$ are regarded as lead reflections with high possibility because they are highly correlated with low height (note that detrended height should be considered here, see Zwally et al. (2008) for details). Therefore, the lowest 2% observations along a 50-km ICESat profile whose waveforms meet at least 2 of the above 4 thresholds are considered to be lead observations during MSS construction. In addition, the proportion of lowest observations is raised from 2% to 4% for Autumn and Summer campaigns, respectively, because the lead fraction of these two seasons confirmed by Cryosat-2 in Section 3.1 is considerably higher than Winters (average lead fractions of 2.9%, 12.8% and 5.7% for March, June and October, respectively). The effectiveness of these modifications is shown in Figure 5. The values of δ_{grid} have been greatly improved after modification, and the values of different campaigns are almost identical.

4. Arctic MSS determined by Cryosat-2 and ICESat

4.1. Mean sea surface model derived by combined Cryosat-2 and ICESat

Since the EGM2008 geoid model has been subtracted from altimetry observations, gridded MDT models are first determined by Cryosat-2 and ICESat exclusively so that the performances of single

altimetry missions can be compared. Lead detection strategies introduced in Section 3 have been applied. Thanks to the dense sampling and high accuracy, the gridded Cryosat-2 MDT can be simply determined by averaging the selected lead measurements in 10-km grids. For ICESat, however, more procedures were needed to overcome the effect of fewer measurements and poorer time resolution. Average height is first calculated in 10-km grids and gaps between ICESat tracks for each campaign are filled by interpolation, and a 25-km half-wavelength Gaussian filter was applied to suppress the short-wave errors. Then the campaign time series of each grid can be obtained and the final MDT was determined by the average of the time series. The MDT revealed by the two single altimetry missions is shown in Figure 7, along with their differences. Although the valid measurements of the two missions are not comparable and the inter-mission bias was not considered, the results presented in Figure 7 have excellent consistency. The spatial patterns revealed by the two missions show a raised dome in the Beaufort Sea caused by Beaufort Gyre and an obvious decreasing trend towards the Atlantic Ocean. Even the small details revealed by the two altimetry missions are similar, such as the stripes close to the Canadian Arctic Archipelago and north to Severnaya Zemlya. Generally, MDT derived from Cryosat-2 seems to be higher in the Beaufort Sea and lower towards the Atlantic Ocean than the one derived from ICESat, perhaps due to different time spans and unsolved bias between the two missions. Anyway, these encouraging results proved that both Cryosat-2 and ICESat can provide reliable information for sea surface studies in ice-covered oceans.

Finally, the Arctic MSS model in the ice-covered region is determined by combining Cryosat-2 and ICESat observations. Before MSS model construction, the bias between Cryosat-2 and ICESat should be removed. Rose et al. (2019) determined inter-mission biases between ERS-1/2, Envisat and Cryosat-2 by calculating the differences in the monthly median of overlapping satellite pairs. However, the two missions we used here didn't coincide in time. Therefore, the bias between ICESat and Cryosat-2 was determined as follows. Firstly, the monthly mean or campaign mean in 10-km grids is calculated for the two missions, and consequently, time series are established. Secondly, the sea level of May 2009 (this epoch is roughly the mean of the time of the last ICESat campaign and the first month of Cryosat-2) is estimated by the extrapolation of both ICESat and Cryosat-2 time series for each grid, and the differences are recorded. An illustration of this procedure is shown in Figure 8, the data of which are extracted from a specific grid located at 126.10°E, 82.41°N. In this case, the bias between the two missions is −5.31 cm, as the double arrow illustrated in Figure 8. Finally, the inter-mission bias is determined as the median of the differences for all the grids. As a result, we found that ICESat observations were 3.87 cm lower than Cryosat-2. Since Cryosat-2 is considered to have better precision according to the result shown in Section 3, a positive 3.87 cm correction was added to all the ICESat lead observations.

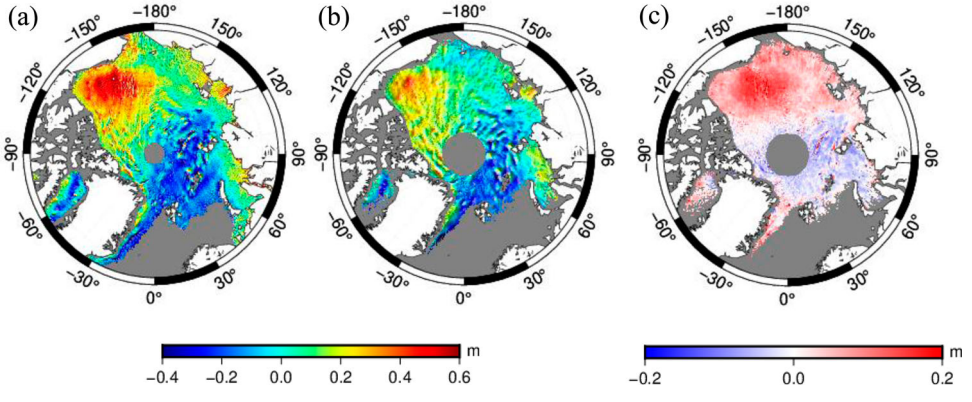

Figure 7. Arctic MDT revealed by (a) Cryosat-2 and (b) ICESat and (c) the difference between them.

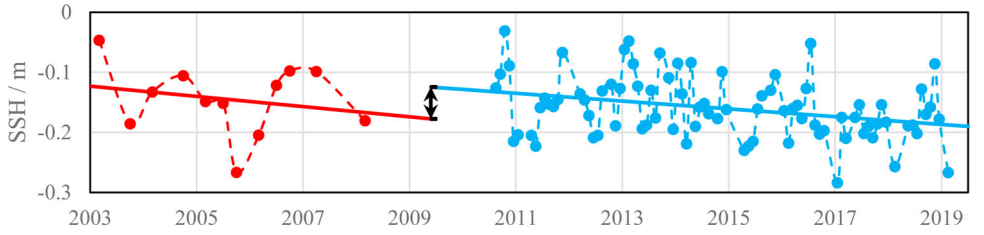

Figure 8. Illustration of inter-mission bias determination in each grid. Red and blue dots represent SSH observed by ICESat and Cryosat-2 respectively, the solid lines show the linear trend captured by the two missions.

Two methods can be used to calculate the mean sea surface. The first method is simply averaging all the available altimetry measurements in each grid. But the result of this method is expected to be very similar to that of Cryosat-2 exclusively because the ICESat observations are much less than those of Cryosat-2, due to the poor time resolution of ICESat compared with Cryosat-2 (13 campaigns versus 105 months in our study). The second method is to establish monthly (campaign) sea level time series for each grid, and the sea level can be referred to as

$$H_i = H_0 + a_{1.} \cdot (t_i - t_0) + a_2 \cdot \sin(2\pi t_i) + a_3 \cdot \cos(2\pi t_i) \tag{4}$$

where Hi is the ith sea level of the time series, t_i is the corresponding time in years, H_0 is the reference sea level at reference time t_0, a1 represents the linear trend of sea level variation, and the trigonometric terms are used to represent seasonal variation, a2 and a3 are the corresponding coefficients. The epoch of 2011.0 (i.e. 0:00 on 1 January 2011), approximately the average epoch of the altimetry missions used in this paper, was chosen as the reference time t_0, and the sea level at this epoch is regarded as the mean sea level of the period. Consequently, the mean sea level can be estimated by least square estimation (LSE) with equation (4). To understand the difference between the two methods, an example is illustrated in Figure 9, with sea surface height (SSH) time series in one 10km-grid centered at 118.46°E, 83.13°N. In this particular grid, the SSH time series consists of 11 ICESat campaign mean SSH and 85 Cryosat-2 monthly mean SSH. The average value of the whole time series is −14.31 cm (green line in Figure 9). This value is much closer to the Cryosat-2 average (−14.99 cm) than the ICESat average (−9.09 cm) because the length of the Cryosat-2 series is almost 8 times the length of the ICESat series. Obviously, the contribution of ICESat observations is very limited in this case. However, when using the LSE method with equation (4), the mean sea level is −11.87 cm as the SSH at the 2011.0 epoch. This is considered to be a more reasonable value because the ICESat observations are better absorbed by the LSE method. Therefore, the LSE method was chosen for mean sea surface calculation and the final MSS model was established after restoring the EGM2008 geoid in each grid. For the convenience of application,

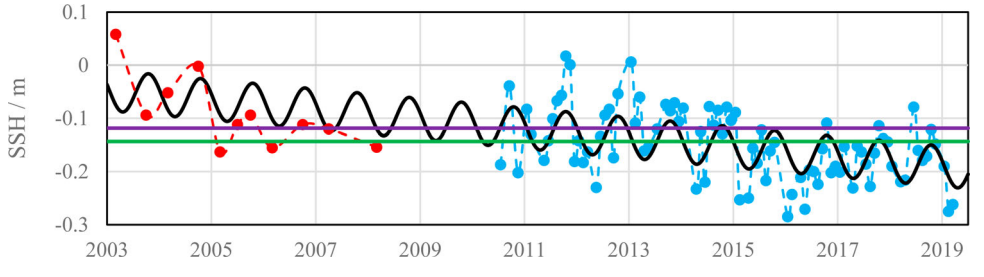

Figure 9. An example of SSH time series in the particular grid located at 118.46°E, 83.13°N. Red and blue dots represent SSH observed by ICESat and Cryosat-2, respectively, the black curve illustrates the simulated SSH determined by Equation (4), and the purple and green line show the mean sea surface determined by simply average and LSE, respectively.

the model is resampled to 2'×2' resolution and named the SUST22 Arctic MSS model, as shown in Figure 10.

4.2. Comparative evaluation of SUST22

To investigate the performance of the SUST22 model, it is first compared with four published MSS models, including DTU21, CLS2015, WHU2013 and UCL2013 MSS within the Arctic. For better comparability, these models are all converted into 2'×2' resolution and referenced to T/P ellipsoid, and the spatial coverage is limited to north of 66°N. Comparisons are made between all five models. However, SUST22 is not directly compared with CLS2015 and WHU2013 because the former only covers the ice-covered region of the Arctic Ocean, while the latter two have large gaps in the central Arctic. Differences between the five MSS models are illustrated in Figure 11 and listed in Table 1.

Firstly, the three global MSS models, DTU21, CLS2015 and WHU2013, are compared with each other as shown in Figure 11(a–c). The three models are almost identical in Bering Strait and between Greenland and the European continent where the Ocean is not or just seasonally covered by sea ice. This is because similar altimetry missions (i.e. ERS-1/2, Envisat and Cryosat-2) were used in this region and careful data processing techniques were applied for open oceans when these three models were established. In perennially ice-covered areas (i.e. the dash line enclosed region in Figure 11(a–f), showing the median sea ice index of September from 1981 to 2010); however, the three models differ from each other. Generally, the difference between DTU21 and CLS2015 seems to be moderate in Figure 11(a), yet a large standard deviation (Std) of 15.7 cm is revealed

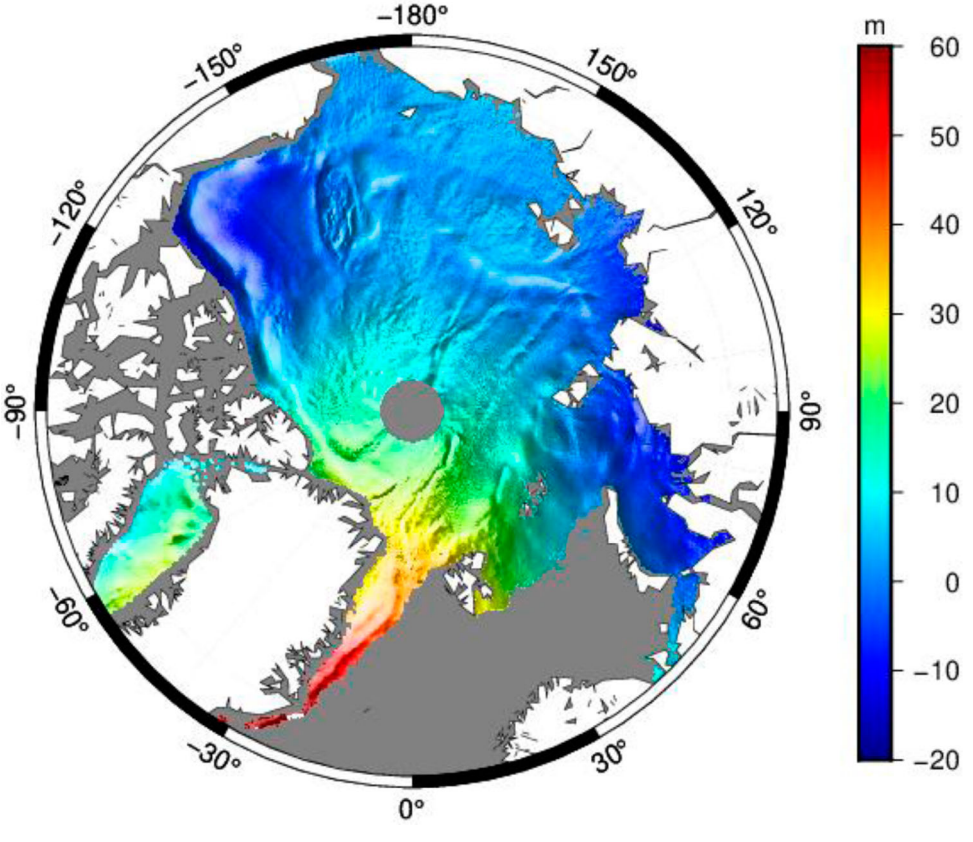

Figure 10. Illustration of the SUST22 MSS model, the height is with respect to T/P Ellipsoid.

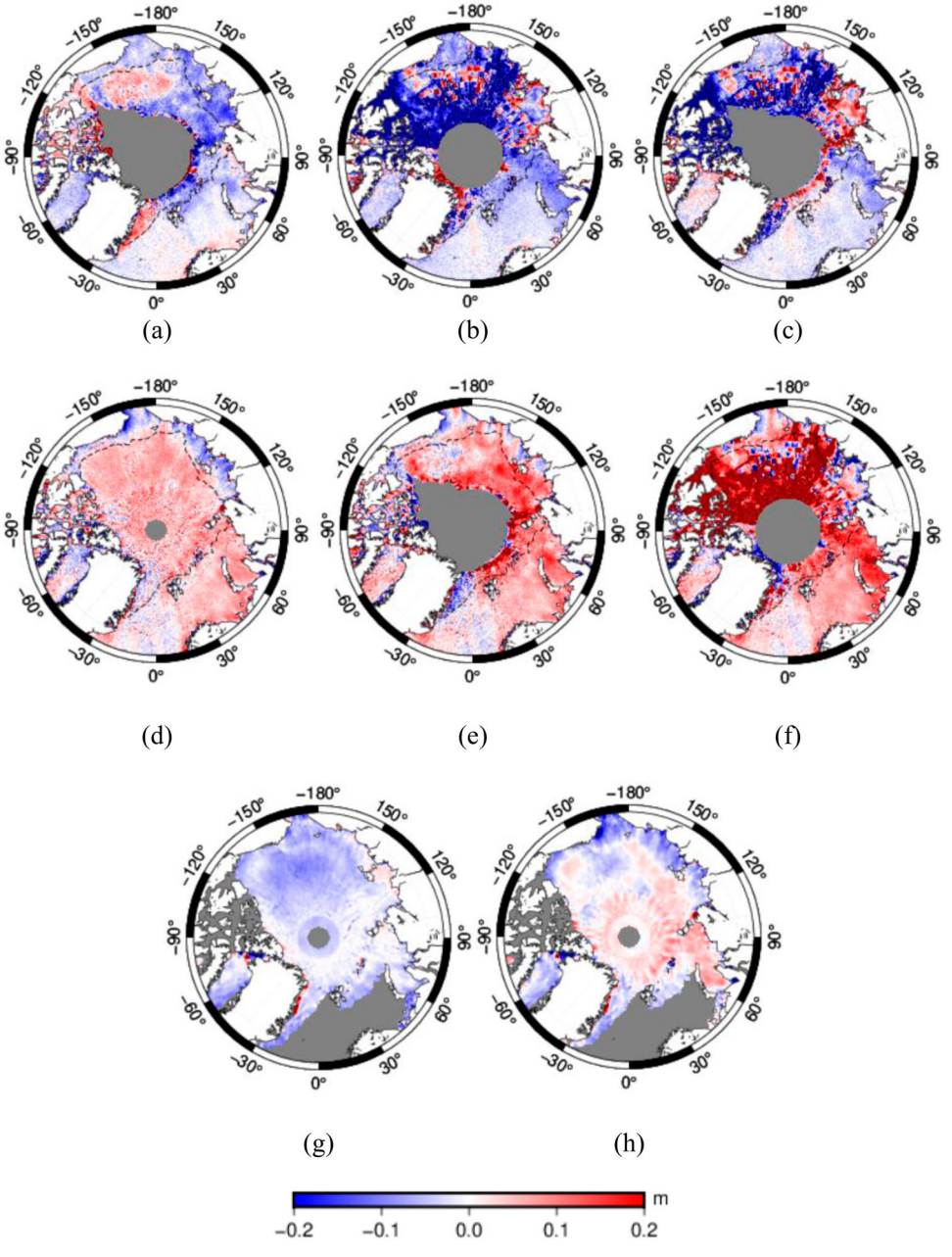

Figure 11. Differences between Arctic MSS models: (a) DTU21-CLS2015, (b) DTU21-WHU2013, (c) CLS2015-WHU2013, (d) DTU21-UCL2013, (e) CLS2015-UCL2013, (f) WHU2013-UCL2013, (g) SUST22-DTU21, (h) SUST22-UCL2013. The dashed lines in (a)-(f) indicate the Median September sea ice index from 1981 to 2010 (Fetterer et al. 2017).

in Table 1. This discrepancy is caused by exaggerated errors at the northern margin of CLS2015, leading to obvious differences around the central Arctic in Figure 11(a). The average difference is reduced to -2.5 ± 6.9 cm between DTU21 and CLS2015 when the comparison area is limited to 83°N, showing excellent consistency between the two models. Large discrepancies are shown between WHU2013 and the other two models, which mainly concentrated in the perennially ice-covered areas. The model is generally higher than the other two (Table 1), which is probably due

Table 1. Statistical results of Arctic MSS model comparison.

Differences	Mean	Std
DTU21-CLS2015	−2.03	15.67
DTU21-WHU2013	−9.32	18.17
CLS2015-WHU2013	−6.02	22.07
DTU21-UCL2013	2.59	8.94
CLS2015-UCL2013	4.26	17.54
WHU2013-UCL2013	11.72	19.97
DTU21-CLS2015(below 83°N)	−2.53	6.91
WHU2013-CLS2015(below 83°N)	5.46	17.55
UCL2013-CLS2015(below 83°N)	−4.78	10.67
SUST22-DTU21	−4.02	5.21
SUST22-UCL2013	−1.05	8.39
		Unit: cm

to the absence of sea ice-specialized data processing. These results have shown that the MSS models in the ice-covered region in the Arctic are less accurate than the open Ocean, highlighting the necessity of the study of Arctic sea level.

Secondly, UCL2013 is compared with DTU21, CLS2015 and WHU2013 MSS models. Due to few data sources compared with the other three models, the differences in open oceans shown in Figure 11(d–f) are more apparent than in Figure 11(a–c). However, a great agreement is shown between DTU21 and UCL2013, with an average difference of 2.6 ± 8.9 cm for the entire Arctic according to Table 1. These two models also have the best spatial coverages in the Arctic among all the five models in this paper, leading to the largest extent shown in Figure 11(d). Again, a large discrepancy is revealed when compared with WHU2013, with an average difference of 11.7 ± 20.0 cm. The difference between CLS2015 and UCL2013 is also large but can be greatly reduced when the comparison area is limited to 83°N.

Finally, SUST22 is compared with DTU21 and UCL2013. Surprisingly, even though the open ocean is not involved, the three models show excellent agreements with each other in the ice-covered region. The 5.2 cm Std of SUST22-DTU21 is the smallest one in Table 1, suggesting that the spatial patterns revealed by these two models are highly similar. The mean difference between SUST22 and DTU21 is 4.0 cm which may be caused by different reference missions. The −1.1 cm mean difference suggests that SUST22 and UCL2013 are the closest models on average among the five. In addition, the 8.4 cm Std is also the second smallest one if the results of CLS2015 (below 83°N) are not considered. Discontinuities at 86°N parallel can be seen in Figure 11(g,h), due to the participation of ICESat in SUST22 and absence in DTU21 and UCL2013. This discontinuity in Figure 11(g) can be greatly improved if 2015.0 is selected as the reference time in the LSE procedure (not shown). This is because DTU21 is determined exclusively by Cryosat-2 north to 81.5°N and the epoch of 2015.0 is more close to the average time of the mission. This also emphasizes the necessity of a longer time span of altimetry data and the effect of the LSE method during MSS construction. Nevertheless, the agreement of the three models, especially the small Std of SUST22-DTU21, turns out that the SUST22 MSS model is reliable.

4.3. Validation by ICESat-2 samples

The SUST22 model is further validated by ICESat-2 observations, together with other four models for comparison. To avoid possible biases caused by seasonal variation of the Arctic sea surface, 12 ICESat-2 tracks from different months were randomly selected in this section, as listed in Table 2. Lead samples from these 12 tracks can be identified by the height_segment_ssh_flag provided in the ATL07 product and finally, 454,224 observations are selected for MSS validation. The mean differences between altimetry samples and the five MSS models are tabulated in Table 3, along with standard deviations (Std). The histograms are shown in Figure 12. Due to the unreliable values at the northern margin, different areas are inspected for CLS2015: full coverage of the model and north to

Table 2. ICESat-2 tracks used for MSS validation.

Year	Month	Day	Cycle nO.	Track ID
2018	Nov	16	01	0753
2019	Jan	24	02	0412
2019	Aug	26	04	0903
2019	Sep	24	04	1349
2020	Feb	28	06	0968
2020	Apr	09	07	0206
2020	Jul	16	08	0321
2020	Dec	20	09	1335
2021	May	02	11	0584
2021	Jun	16	11	1271
2021	Oct	25	13	0503
2022	Mar	04	14	1098

Table 3. Differences between MSS models and altimetry samples.

MSS models	ICESat-2 samples	
	Mean	Std
SUST22	15.79	7.42
DTU21	12.30	8.05
CLS2015	10.00	30.54
WHU2013	−0.01	17.71
UCL2013	15.23	8.58
CLS2015 (below 83°N)	8.32	14.29
	Unit: cm	

83°N. Inter-mission biases are not considered here for ICESat and ICESat-2 samples, hence the Std is a more persuasive indicator than the mean difference in Table 3.

Generally, the accuracy of SUST22 can be guaranteed with the smallest Std of 7.42 cm, which means it captures more reliable characteristics of the spatial distribution of the Arctic sea surface. However, the 15.79 cm mean difference is the largest in Table 3. This is probably due to the inter-mission bias between Cryosat-2 and ICESat-2 because a similar difference is shown between UCL2013 and ICESat-2 Samples. The histogram shown in Figure 12(a) is close to the normal distribution, which also gives us confidence that the model is seldom affected by gross errors. From the view of Std, DTU21 and UCL2013 both show similar behaviors to SUST22, while CLS2015 and WHU2013 show large Stds according to ICESat-2 validation. DTU21 MSS shows the second smallest Std value of 8.05 cm. This model is expected to have a good performance because it includes more satellite altimetry missions than SUST22 and is more recently released than the other three models. The performance of UCL2013 is beyond expectation because the data source of this model consists of only two complete cycles of Cryosat-2, which is much less than the other models. CLS2015 shows the largest Std of 30.54 cm due to the unreliable values at the north margin of the model. This is also revealed by the asymmetric histogram shown in Figure 12(c). When the area is limited to below 83°N, the Std has been greatly improved for CLS2015 but is still not comparable with SUST22, DTU21 and UCL2013. The performance of WHU2013 is not ideal in the ice-covered Arctic according to the 17.71 cm Std and the messy distribution in the histogram (The axis ranges of Figure 12(d) are different from others since there are too many outliers in the WHU2013 model).

5. Discussions

5.1. Variation of ICESat waveform character

In most of the Arctic Ocean and sea ice studies using ICESat, the lowest-level method was implemented for lead detection. However, the waveform of laser altimetry can also reveal the characteristics of the reflected surface and provide valuable information for lead detection, like

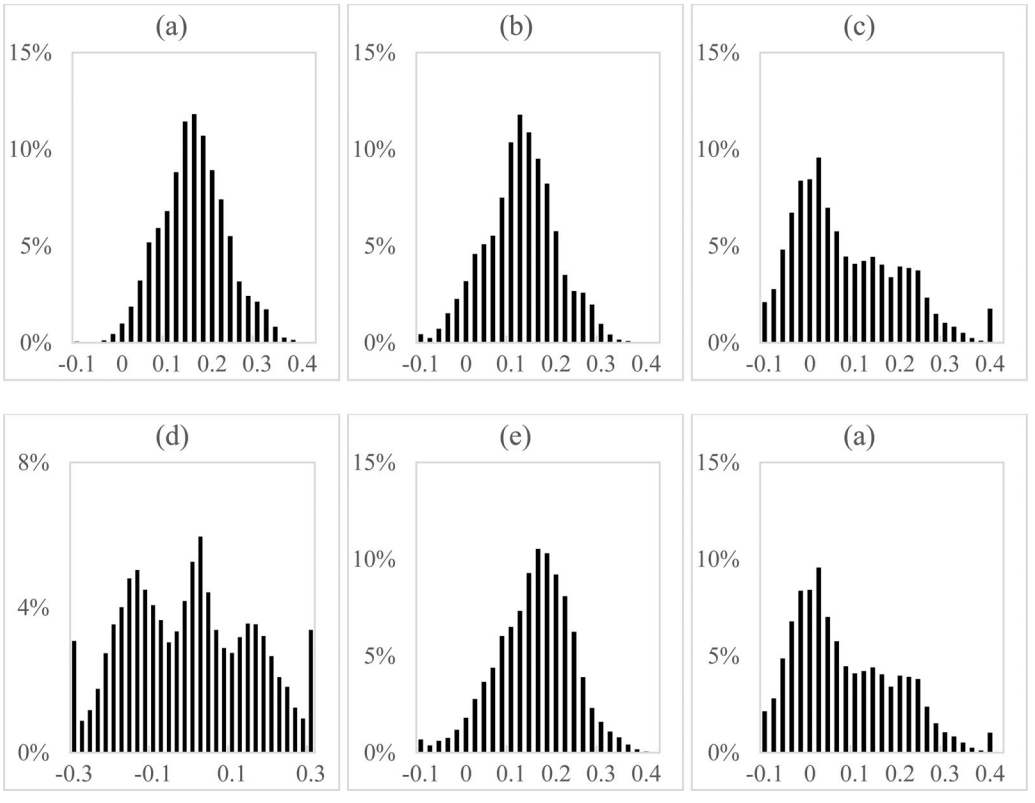

Figure 12. Histograms of the differences between ICESat-2 samples and (a) SUST22, (b) DTU21, (c) CLS2015, (d) WHU2013, (e) UCL2013 and (f) CLS2015 (below 83°N)

the editing procedure used in Section 3.2. Some research studies identified leads by waveform independently (e.g. Farrell et al. 2009). The waveform parameters are also used for the quality control of ICESat measurements. Usually, these works were done with fixed thresholds of waveform parameters for every campaign. However, the features of the ICESat waveform may change with campaigns according to our study. More specifically, it may be related to the energy attenuation of ICESat lasers. Figure 13 illustrates the average values of the four parameters used in this study for each campaign, dots of different colors represent different lasers. Notable trends related to time can be observed for all four parameters, especially those campaigns implemented with laser 3 (blue dots in Figure 13). Receiver gain (G) shows the clearest pattern among the four parameters. By the end of the laser 3 period (campaign 08FM), its average value had fallen to about one-third of the first campaign of the laser (04ON). Reflectivity (R) and pulse broadening (S) also change with time, the former shows an uptrend and the latter shows a downtrend. Strong correlations are found between the average values of these three parameters. When the whole ICESat period is considered, the correlation coefficients are 0.59 between G and R and 0.65 between G and S. If only the period of laser 3 is considered, the correlation coefficients increase to 0.66 and 0.82, respectively. The trend of the length of the received waveform is less noticeable, but there is also a correlation coefficient of 0.43 between G and L. The most reasonable explanation for these time-related variations is the energy attenuation due to manufacturing defects of the lasers. To prove this, the average values of the waveform parameters during campaign 03FM are inspected daily, as shown in Figure 14. 03FM was the first campaign of ICESat, it was implemented with laser 1 continuously until the laser broke down. Similar to Figure 13, clear trends are observed in the variation of G, S and L during the implementation period of laser 1. Although the R variation of FM03 shows no obvious

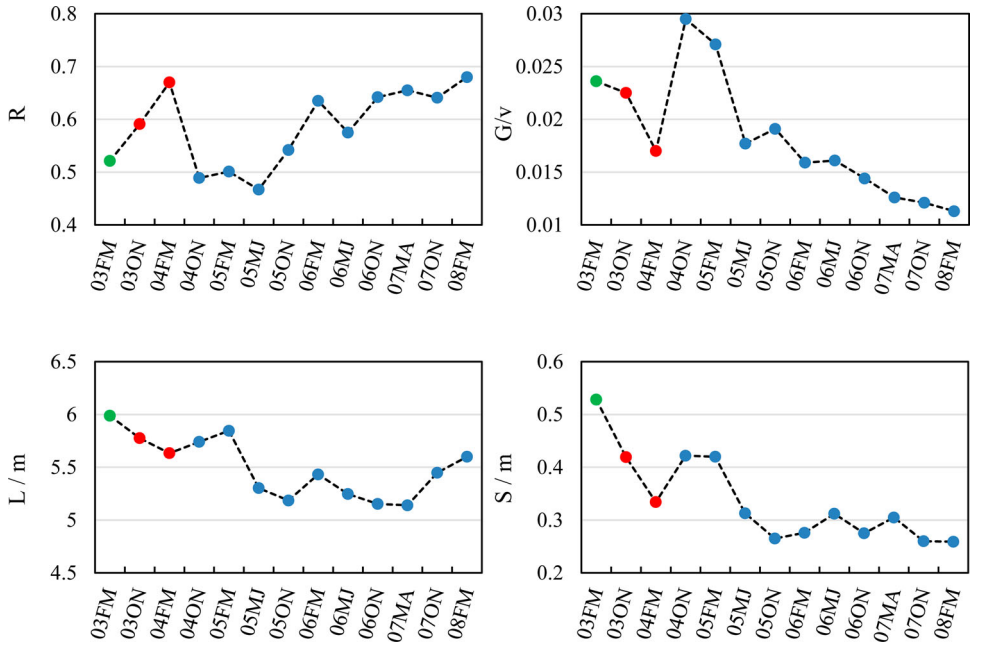

Figure 13. Average values of R, G, L and S for each ICESat campaign. Different colors denote the laser operated in each campaign, green, red and blue for laser 1,2 and 3, respectively.

pattern, the results shown in Figure 13 and Figure 14 are enough to conclude that the ICESat waveform can be affected by laser energy.

This impact is problematic for those procedures that rely on waveform parameters. For example, Farrell et al. (2009) utilized a receiver gain threshold of 30 counts (0.03v) to eliminate those measurements affected by atmospheric scattering. However, according to our test, this procedure

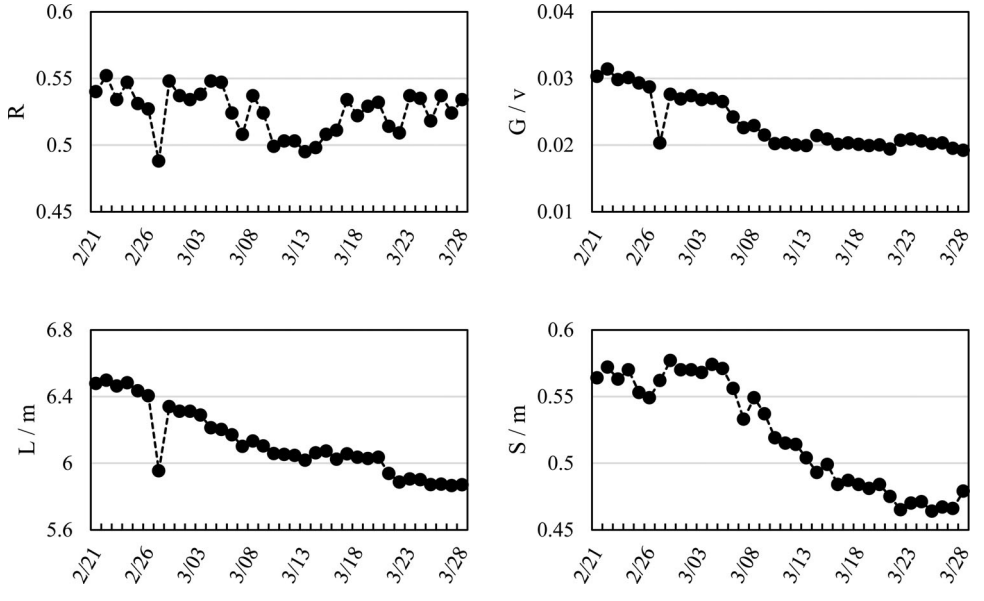

Figure 14. Average values of R, G, L and S for each day in campaign 03FM, which was operated by laser 1.

would reject more than 30% of data for campaigns 04ON and 05FM and more than 20% for 03FM and 03ON, while less than 1% of data would be rejected for the other campaigns. This difference is more likely caused by the variation of receiver gain itself (see Figure 13 top right) because it is difficult to believe that the condition of the Arctic Ocean had such drastic changes. Therefore, maybe flexible parameter thresholds are better than fixed values for ICESat quality control and lead detection. However, it needs more research, hence fixed thresholds were still implemented in this paper.

5.2. Performance over the ice-covered ocean: ICESat versus Cryosat-2

Due to the flatness of the Arctic Ocean on a small scale and short term, the standard deviation of sea surface height determined by identified lead observations is considered to be an indicator of the quality of altimetry records. The median δ_{grid} values of Cryosat-2 lead observations in each month have been shown in Figure 4, the average value of around 3.5 cm indicates the good lead detection ability of Cryosat-2. The δ_{grid} values of ICESat-derived lead observations have been shown in Figure 5. The values obtained with the original 2% lowest-level method were not ideal but have been greatly improved after the modification, especially those campaigns before 06ON. However, the average δ_{grid} value of about 5 cm of ICESat (after modification) is still inferior to that of Cryosat-2.

It is also worth noting that Cryosat-2 can observe leads than ICESat. For example, about 6.1% of the Cryosat-2 observations were identified as leads on average in March when the thresholds of PP > 70 and SSD < 3 were implemented, while the proportion for ICESat lead measurements in FM campaigns is only 1.2% with the lead detection procedure adopted in Section 3.2. Examples of both missions are displayed in Figure 15. One may argue that few lead observations detected from ICESat data are mainly caused by the lowest-level strategy. However, a higher proportion in the lowest-level method will lead to an increased risk that sea ice observations may be misidentified as leads and contaminate the sea surface height estimation. Besides, Farrell et al. (2009) implemented a lead detection method completely based on the waveform and identified only 0.5% of ICESat observations as leads for campaign FM05, which was even less than the lowest-level method.

In addition, Cryosat-2 also has a better resolution than ICESat, which not only has obvious advantages in time resolution but also has higher spatial resolution due to dense orbits. Therefore,

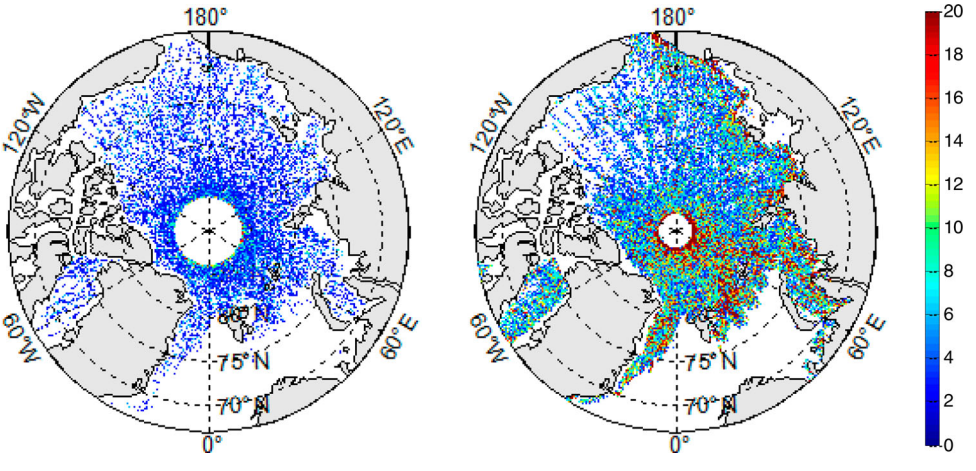

Figure 15. Numbers of identified lead observations in each grid of ICESat in the 05FM campaign (left) and Cryosat-2 in March 2017.

Cryosat-2 is strongly recommended for studies in the Arctic ice-covered ocean if only one altimetry mission is needed. However, ICESat provides unique data above 81.5°N during 2003–2009, hence is still indispensable for a comprehensive understanding of the Arctic Ocean and sea ice.

6. Summary

In this paper, a new Arctic MSS model named SUST22 is established by combined Cryosat-2 and ICESat observations. Our interest focuses on the ice-covered regions because these two missions have higher latitudinal coverages than traditional altimetry satellites. The lead detection strategies for both missions were optimized. The results show that both missions can provide reliable sea surface height with similar standard deviations of around 3–5 cm within 10-km grids in a month. Then the process of MSS model construction is discussed. Lead observations derived from the altimetry missions are first separated into 10-km grids for each month, then the new SUST22 MSS is determined by LSE of the sea surface time series in each grid. This model can be downloaded from https://www.scidb.cn/anonymous/QnZFRmZt in a form of a 2'×2' resolution grid.

The accuracy and reliability of SUST22 is investigated by comparing it with other four MSS models including DTU21, CLS2015, WHU2013 and UCL2013, and validated by altimetry samples from Cryosat-2, ICESat and ICESat-2 missions. Among the five MSS models, SUST22, DTU21 and UCL2013 MSS seem to be more reliable in the Arctic because they have good agreement with each other and altimetry samples. DTU21 and UCL2013 models also have better spatial coverages than the other three. Despite the biases due to different references, the standard deviations between these models are typically over 5 cm, even at the decimeter level. This is not comparable to the mid-low regions where usually a few centimeter level standard deviations are found for different models (Jin, Li, and Jiang 2016). There are fewer available altimetry observations in polar regions than in the open oceans, and the time span is much shorter. Moreover, the sophisticated technologies used for mid-low latitude oceans are not suitable for polar oceans due to sea ice. Therefore, the construction of high-accuracy polar MSS model is still challenging. Generally, more observations and longer time series are needed to improve the accuracy and resolution of the MSS model. This is also why full play to the role of ICESat data was given in the SUST22 construction procedure even though the ICESat observations are considered to be less accurate than those of Cryosat-2. For the same reason, other missions, such as ERS-1/2, Envisat and ICESat-2, are also needed to achieve better accuracy. However, the intermission biases, sea level variation, seasonal signals and orbit errors should be carefully considered when combining multi-mission data. Despite these problems, the -4.0 ± 5.2 cm difference between SUST22 and DTU21 is much better than the differences between any other models, indicating the possibility of the construction of a high-accuracy MSS model.

Acknowledgements

The authors thank ESA for providing CryoSat-2 products and NSIDC for providing ICESat, ICESat-2 and MODIS products.

Disclosure statement

No potential conflict of interest was reported by the author(s).

Funding

This work was supported by the National Natural Science Foundation of China [grant numbers 421932511 and 41804002], the Open Research Foundation of the Key Laboratory of Geospace Environment and Geodesy, the Ministry of Education, Wuhan University [grant number 19-01-04], and the Special Fund of Hubei Luojia Laboratory [grant number 220100003].

ORCID

Guodong Chen http://orcid.org/0000-0002-4086-8504

References

Abshire, J. B., X. Sun, H. Riris, J. M. Sirota, J. F. McGarry, S. Palm, D. Yi, and P. Liiva. 2005. "Geoscience Laser Altimeter System (GLAS) on the ICESat Mission: On-Orbit Measurement Performance." *Geophysical Research Letters* 32: L21S02. doi:10.1029/2005GL024028.

Andersen, O. B., A. Abulaitijiang, S. Zhang, and K. S. Rose. 2021. "A New High Resolution Mean Sea Surface (DTU21MSS) for Improved Sea Level Monitoring." *EGU General Assembly Conference Abstracts, EGU21-16084*.

Andersen, O. B., and P. Knudsen. 2009. "DNSC08 Mean Sea Surface and Mean Dynamic Topography Models." *Journal of Geophysical Research: Oceans* 114 (C11): 1–12. doi:10.1029/2008JC005179.

Andersen, O. B., and G. Piccioni. 2016. "Recent Arctic Sea Level Variations from Satellites." *Frontiers in Marine Science* 3(76): 1–6. doi:10.3389/fmars.2016.00076.

Armitage, T. W. K., S. Bacon, A. L. Ridout, S. F. Thomas, Y. Aksenov, and D. Wingham. 2016. "Arctic Sea Surface Height Variability and Change from Satellite Radar Altimetry and GRACE, 2003–2014." *Journal of Geophysical Research: Oceans* 121 (6): 4303–4322. doi:10.1002/2015JC011579.

Brenner, A. C., J. P. DiMarzio, and H. J. Zwally. 2007. "Precision and Accuracy of Satellite Radar and Laser Altimeter Data Over the Continental Ice Sheets." *IEEE Transactions on Geoscience and Remote Sensing* 45 (2): 321–331. doi:10.1109/TGRS.2006.887172.

Cheng, Y., O. B. Andersen, and P. Knudsen. 2015. "An Improved 20-Year Arctic Ocean Altimetric Sea Level Data Record." *Marine Geodesy* 38 (2): 146–162. doi:10.1080/01490419.2014.954087.

Connor, L. N., S. W. Laxon, A. L. Ridout, W. B. Krabill, and D. C. McAdoo. 2009. "Comparison of Envisat Radar and Airborne Laser Altimeter Measurements Over Arctic Sea Ice." *Remote Sensing of Environment* 113 (3): 563–570. doi:10.1016/j.rse.2008.10.015.

Dettmering, D., A. Wynne, F. L. Müller, M. Passaro, and F. Seitz. 2018. "Lead Detection in Polar Oceans – A Comparison of Different Classification Methods for Cryosat-2 SAR Data." *Remote Sensing* 10 (1190): 1–17. doi:10.3390/rs10081190.

Doglioni, F., R. Ricker, B. Rabe, and T. Kanzow. 2022. "Sea Surface Height Anomaly and Geostrophic Current Velocity from Altimetry Measurements Over the Arctic Ocean (2011–2020)." *Earth System Science Data Discussions* 170: 1–46. doi:10.5194/essd-2021-170.

Farrell, S. L., S. W. Laxon, D. C. McAdoo, D. Yi, and H. J. Zwally. 2009. "Five Years of Arctic Sea Ice Freeboard Measurements from the Ice, Cloud and Land Elevation Satellite." *Journal of Geophysical Research* 114: C04008. doi:10.1029/2008JC005074.

Farrell, S. L., D. C. McAdoo, S. W. Laxon, H. J. Zwally, D. Yi, A. Ridout, and K. Giles. 2012. "Mean Dynamic Topography of the Arctic Ocean." *Geophysical Research Letters* 39: L01601. doi:10.1029/2011GL050052.

Fetterer, F., K. Knowles, W. N. Meier, M. Savoie, and A. K. Windnagel. 2017. Data from: Sea Ice Index, Version 3". NSIDC: National Snow and Ice Data Centre. Accessed May 15, 2022. https://nsidc.org/data/G02135/versions/3.

Forsberg, R., and H. Skourup. 2005. "Arctic Ocean Gravity, Geoid and Sea-ice Freeboard Heights from ICESat and GRACE." *Geophysical Research Letters* 32: L21502. doi:10.1029/2005GL023711.

Guerreiro, K., S. Fleury, E. Zakharova, A. Kouraev, F. Remy, and P. Maisongrande. 2017. "Comparison of CryoSat-2 and ENVISAT Radar Freeboard Over Arctic Sea Ice: Toward An Improved Envisat Freeboard Retrieval." *The Cryosphere* 11 (5): 2059–2073. doi:10.5194/tc-11-2059-2017.

Jin, T., J. Li, and W. Jiang. 2016. "The Global Mean Sea Surface Model WHU2013." *Geodesy and Geodynamics* 7: 202–209. doi:10.1016/j.geog.2016.04.006.

Kwok, R., G. F. Cunningham, H. J. Zwally, and D. Yi. 2007. "Ice, Cloud, and Land Elevation Satellite (ICESat) Over Arctic Sea Ice: Retrieval of Freeboard." *Journal of Geophysical Research* 112: C12013. doi:10.1029/2006JC003978.

Kwok, R., and J. Morison. 2011. "Dynamic Topography of the Ice-covered Arctic Ocean from ICESat." *Geophysical Research Letters* 38 (2): 79–89. doi:10.1029/2010GL046063.

Laxon, S. W., K. A. Giles, A. L. Ridout, D. J. Wingham, R. Willatt, R. Cullen, R. Kwok, et al. 2013. "CryoSat-2 Estimates of Arctic Sea Ice Thickness and Volume." *Geophysical Research Letters* 40 (4): 732–737. doi:10.1002/GRL.50193.

Lee, S., H. Kim, and J. Im. 2018. "Arctic Lead Detection Using A Waveform Mixture Algorithm from CryoSat-2 Data." *The Cryosphere* 12 (5): 1665–1679. doi:10.5194/tc-12-1665-2018.

Pavlis, N. K., S. A. Holmes, S. C. Kenyon, and J. K. Factor. 2012. "The Development and Evaluation of the Earth Gravitational Model 2008 (EGM2008)." *Journal of Geophysical Research: Solid Earth* 117 (B4). doi:10.1029/2011JB008916.

Peacock, N. R., and S. W. Laxon. 2004. "Sea Surface Height Determination in the Arctic Ocean from ERS Altimetry." *Journal of Geophysical Research: Oceans* 109 (C7): 1–14. doi:10.1029/2001JC001026.

Poisson, J. C., G. D. Ouartly, A. A. Kurekin, P. Thibaut, D. Hoang, and F. Nencioli. 2018. "Development of An ENVISAT Altimetry Processor Providing Sea Level Continuity Between Open Ocean and Arctic Leads." *IEEE Transactions on Geoscience and Remote Sensing* 56 (9): 5299–5318. doi:10.1109/TGRS.2018.2813061.

Prandi, P., M. Ablain, A. Cazenave, and N. Picot. 2012. "A New Estimation of Mean Sea Level in the Arctic Ocean from Satellite Altimetry." *Marine Geodesy* 35 (sup1): 61–81. doi:10.1080/01490419.2012.718222.

Prandi, P., J. C. Poisson, Y. Faugère, A. Guillot, and G. Dibarboure. 2021. "Arctic Sea Surface Height Maps from Multi-altimeter Combination." *Earth System Science Data* 13 (12): 5469–5482. doi:10.5194/essd-13-5469-2021.

Ricker, R., S. Hendricks, V. Helm, H. Skourup, and M. Davidson. 2014. "Sensitivity of CryoSat-2 Arctic Sea-ice Freeboard and Thickness on Radar-Waveform Interpretation." *The Cryosphere* 8 (4): 1607–1622. doi:10.5194/tc-8-1607-2014.

Rose, S. K., O. B. Andersen, M. Passaro, C. A. Ludwigsen, and C. Schwatke. 2019. "Arctic Ocean Sea Level Record from the Complete Radar Altimetry Era: 1991–2018." *Remote Sensing* 11 (1672): 1–29. doi:10.3390/rs11141672.

Schaeffer, P., Y. Faugére, J. F. Legeais, A. Ollivier, T. Guinle, and N. Picot. 2012. "The CNES_CLS11 Global Mean Sea Surface Computed from 16 Years of Satellite Altimeter Data." *Marine Geodesy* 35 (sup1): 3–19. doi:10.1080/01490419.2012.718231.

Skourup, H. 2009. "A Study of Arctic Sea Ice Freeboard Heights, Gravity Anomalies and Dynamic Topography from ICESat Measurements." PhD diss., University of Copenhagen.

Skourup, H., S. L. Farrell, S. Hendricks, R. Ricker, T. W. K. Armitage, A. Ridout, O. B. Andersen, C. Hass, and S. Baker. 2017. "An Assessment of State-of-the-art Mean Sea Surface and Geoid Models of the Arctic Ocean: Implications for Sea Ice Freeboard Retrieval." *Journal of Geophysical Research: Oceans* 122 (11): 8593–8613. doi:10.1002/2017JC013176.

Spreen, G. 2008. "Satellite-based Estimates of Sea Ice Volume Flux: Applications to the Fram Strait Region." PhD diss., University of Hamburg.

Sun, W., X. Zhou, L. Yang, D. Zhou, and F. Li. 2021. "Construction of the Mean Sea Surface Model Combined HY-2A With DTU18 MSS in the Antarctic Ocean." *Frontiers in Environmental Science* 9(697111): 1–9. doi:10.3389/fenvs.2021.697111.

Tilling, R., A. Ridout, and A. Shepherd. 2019. "Assessing the Impact of Lead and Floe Sampling on Arctic Sea Ice Thickness Estimates from Envisat and CryoSat-2." *Journal of Geophysical Research: Oceans* 124 (11): 7473–7485. doi:10.1016/j.asr.2017.10.051.

Wang, Y. M. 2001. "GSFC00 Mean Sea Surface, Gravity Anomaly, and Vertical Gravity Gradient from Satellite Altimeter Data." *Journal of Geophysical Research: Oceans* 106 (C12): 31167–31174. doi:10.1029/2000JC000470.

Wernecke, A., and L. Kaleschke. 2015. "Lead Detection in Arctic Sea Ice from CryoSat-2: Quality Assessment, Lead Area Fraction and Width Distribution." *The Cryosphere* 9 (5): 1955–1968. doi:10.5194/tc-9-1955-2015.

Wingham, D. J., C. R. Francis, S. Baker, C. Bouzinac, D. Brockley, R. Cullen, P. Chateau-Thierry, et al. 2006. "CryoSat: A Mission to Determine the Fluctuations in Earth's Land and Marine Ice Fields." *Advances in Space Research* 37 (4): 841–871. doi:10.1016/j.asr.2005.07.027.

Zwally, H. J., D. Yi, R. Kwok, and Y. Zhao. 2008. "ICESat Measurements of Sea Ice Freeboard and Estimates of Sea Ice Thickness in the Weddell Sea." *Journal of Geophysical Research* 113: C02S15. doi:10.1029/2007JC004284.